


## Extinction and recovery of mass flow through solid $^4\text{He}$ samples

Jaeho Shin  and Moses H. W. Chan <sup>\*</sup>

*Department of Physics, The Pennsylvania State University, University Park, Pennsylvania 16802-6300, USA*

 (Received 8 September 2019; revised manuscript received 18 November 2019; published 9 January 2020; corrected 19 March 2020)

Superfluidlike mass flow through 2 cm thick solid  $^4\text{He}$  samples sandwiched between two porous Vycor glass rods filled with superfluid was observed in 2008. The flow commences below 0.6 K, increases in magnitude with decreasing temperature, and shuts off abruptly below a temperature  $T_d$  near 0.1 K.  $T_d$  is found to increase with  $^3\text{He}$  impurities at the few parts per million level. The mass flow phenomenon is recently reproduced in  $8\ \mu\text{m}$  thick solid samples; however, the shutoff of mass flow at low temperature is not seen. Here, we report measurements on 2.5 mm thick solid samples. Mass flow rate reduction and extinction near 0.1 K is found only when the concentration of the helium gas,  $X_3$ , used to prepare the sample exceeds respectively  $3.5 \times 10^{-4}$  and  $2 \times 10^{-3}$ . After the extinction, the mass flow shows a gradual but complete recovery with a characteristic time of many hours. The experimental evidence allows us to formulate a model that explains both the extinction and recovery phenomena. The extinction of the mass flow is due to the trapping of  $^3\text{He}$  atoms at the nodes or the intersections of the dislocation network which blocks the transport of  $^4\text{He}$  along the network. The slow recovery in the 2.5 mm samples is due to the migration of the trapped  $^3\text{He}$  atoms along the dislocation lines and drain into the superfluid inside the porous Vycor glass. Our model also explains naturally the absence of mass flow extinction in the  $8\ \mu\text{m}$  samples and the apparent absence of recovery in the 2 cm samples.

DOI: [10.1103/PhysRevB.101.014507](https://doi.org/10.1103/PhysRevB.101.014507)

### I. INTRODUCTION

In 2008 Ray and Hallock of the University of Massachusetts (UMass) reported the remarkable observation that when a 2 cm thick solid  $^4\text{He}$  sample is placed between two porous Vycor glass rods filled with superfluid,  $^4\text{He}$  atoms can be induced to flow across this superfluid-solid-superfluid (*SF-S-SF*) sandwich below 0.6 K [1–3]. Such a *SF-S-SF* experimental configuration is possible because the melting pressure of liquid  $^4\text{He}$  in the porous Vycor glass, owing to the nanometer size pore structure, is elevated by 10 bar to 35 bar. The mass flow rate increases with decreasing temperature and ends abruptly from the maximum value to zero over a narrow temperature range at a temperature  $T_d$  near 0.1 K for samples prepared with gas mixture with  $X_3$  that exceeds  $4 \times 10^{-6}$  [2].  $T_d$  is found to shift to higher temperature with an increase in  $X_3$ . For solid samples prepared with helium gas of  $X_3 = 1.7 \times 10^{-7}$  the extinction of mass flow is not complete. The UMass group proposed that the mass flow is a consequence of transport of  $^4\text{He}$  atoms along dislocation line with superfluid core [4,5]. The understanding of the mass flow extinction phenomenon to date is not as definite, it is thought that the extinction is related to either the binding of  $^3\text{He}$  atoms along the dislocation lines or more specifically at the intersections of the dislocation network.

Many features of the UMass experiment have been confirmed by us in two separate experiments on solid samples of  $8\ \mu\text{m}$  and 2.5 mm in thickness [6,7]. Our study on 2.5 mm thick solid samples, carried out in five sample cells of different designs, verifies the proposal of UMass's group by establish-

ing a direct causal relation between mass flow and dislocation network in the solid; specifically we show mass flow takes place through, instead of around, the solid sample contrary to that suggested by an experiment at the University of Alberta [8] and that no mass flow can be found in solid samples grown inside silica aerogel missing a dislocation network. The other significant findings include the following. (1) In contrast to the results from UMass where mass flow is found only in some samples, mass flow is always found below 1 K near the melting pressure. The region showing mass flow is found to extend to at least 30 bar with a concomitant decrease in the onset temperature down to 0.25 K. (2) The mass flow rate at a fixed temperature, e.g., at 0.1 K, decays exponentially with pressure of the solid sample. (3) The flow rates from the 2 cm, 2.5 mm, and  $8\ \mu\text{m}$  thick samples show a logarithmic decrease with the thickness of the solid samples.

Surprisingly, we found no evidence of any mass flow extinction or even reduction at low temperature in  $8\ \mu\text{m}$  solid samples grown with helium gas of  $X_3$  between  $5 \times 10^{-12}$  and  $1.5 \times 10^{-2}$ . Instead, we found mass flow rate increases smoothly with decreasing temperature from 0.9 K down to 65 mK (see the Supplemental Materials section of Ref. [6]).

### II. EXPERIMENTAL METHOD

In order to understand the contrasting results in the mass flow extinction phenomenon in the 2 cm and  $8\ \mu\text{m}$  samples, we carried out measurements on solid samples of 2.5 mm in thickness in a sample cell known as *C-R* in Ref. [7]. The sample cell (Fig. 1) has the usual *SF-S-SF* geometry. The solid sample is housed within a cylindrical space between two mating flanges that are sealed and thermally anchored to the mixing chamber of the dilution refrigerator. For ease

<sup>\*</sup>Corresponding author: MHC2@psu.edu

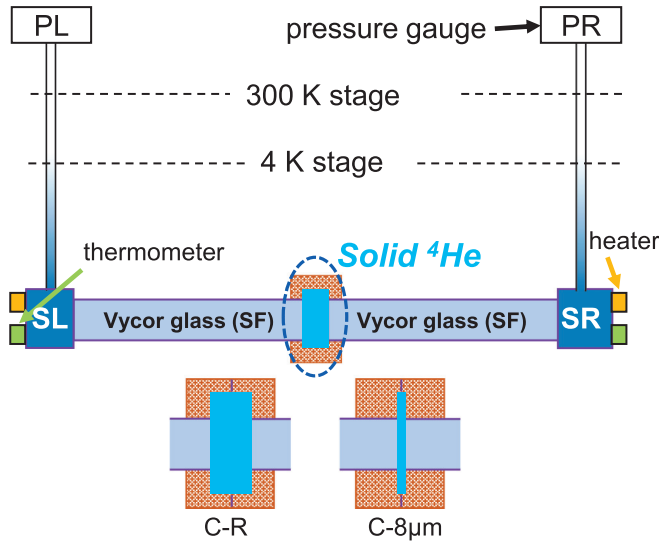


FIG. 1. Schematic drawing of the superfluid-solid-superfluid sandwiched cell *C-R* used in this experiment. Solid sample space with a thickness of 2.5 mm is sandwiched by two porous glass rods with superfluid.

of discussions for the rest of this paper, we will refer to the center of the sample cell holding the solid sample as the “cell body” in contrast to “sample cell,” which refers to the entire *SF-S-SF* assembly. Two porous Vycor glass rods, which serve as superfluid reservoirs, are inserted and sealed on the opposite ends of the cell body. The diameter and length of the Vycor rods are 4.6 mm and 40 mm, respectively. The high temperature ends of the porous Vycor glass rods, regulated near 1.5 K, are sealed with small copper caps with small empty spaces to serve as bulk superfluid reservoirs, *SL* and *SR*, on the left and right side of the *SF-S-SF* sandwich. Two separate thin stainless-steel capillaries connect *SL* and *SR* to the room temperature gas handling system. The inner diameter (I.D.) and length of the capillaries connecting the sample cell to junctions near  $\sim 2.5$  K are respectively 0.1 mm and 1 m. Capillaries with I.D. of 0.4 mm and length of 2 m are used from 2.5 K to room temperature. A chemical potential difference, i.e., superfluid fountain pressure across the *SF-S-SF* sandwich is generated to induced mass flow by imposing a temperature difference between *SL* and *SR*. The total amount of liquid and solid helium in the sample cell are respectively 0.4 and 0.35 cm<sup>3</sup> in volume, containing  $1.79 \times 10^{-2}$  and  $1.68 \times 10^{-2}$  moles of <sup>4</sup>He. The amount of helium gas contained in the room temperature gas handling system and the capillaries is about 2.5% of the helium in the *SF-S-SF* sample cell.

Prior to cool down the sample cell is evacuated with a turbomolecular pump and flushed multiple times with ultrahigh-purity grade (99.999% pure) <sup>4</sup>He gas of  $X_3 = 3 \times 10^{-7}$ . Mass flow measurements were carried out sequentially on samples with progressively higher  $X_3$ . To prepare a solid sample of a new  $X_3$  the sample cell is warmed to 2.5 K and evacuated for 12 h with the turbomolecular pump. Gas mixture is prepared by mixing <sup>4</sup>He gas with  $X_3 = 3 \times 10^{-7}$  and pure <sup>3</sup>He gas at room temperature and then introduced to the sample cell with the cell body thermally anchored at 0.5 K and the high

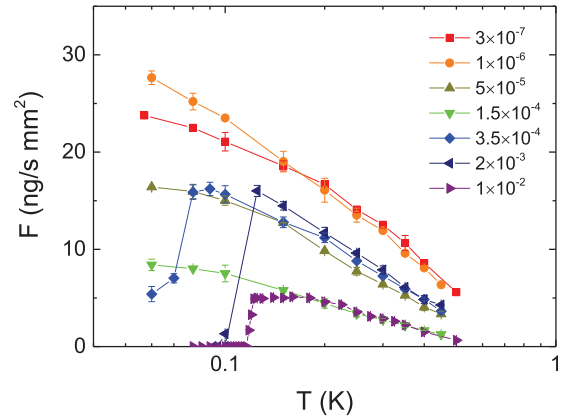


FIG. 2. Temperature dependence of the mass flow rates of solid samples grown with <sup>4</sup>He gas with different  $X_3$ . The thickness of the solid samples is 2.5 mm.

temperature ends of the Vycor rods kept at 1.5 K. Both capillaries on the left and the right of the sample cell are used to bring mixture gas through the Vycor glass into the cell body to condense a superfluid sample near 24 bar. A small pressure gradient of  $\sim 0.2$  bar is maintained between the two capillaries while crossing the <sup>4</sup>He melting boundary to complete the growth of the solid sample at the desired pressure. This procedure was used in Ref. [7] and we have been successful in consistently growing low  $X_3$  solid samples with mass flow. It typically takes 5 to 6 h to grow a solid sample with this procedure.

### III. EXPERIMENTAL RESULTS

Figure 2 shows mass flow rate as a function of temperature for solid samples prepared with gas mixture of different  $X_3$ . The mass flow rate is normalized by the cross-sectional area of the Vycor rods and expressed in units of nanogram of <sup>4</sup>He per s per mm<sup>2</sup> or ng/s mm<sup>2</sup>. The data points on each curve were measured and recorded at 15 min intervals. Samples made with gas mixture with  $X_3$  at and below  $1.5 \times 10^{-4}$  show flow rate that increases smoothly with decreasing temperature down to 60 mK without any sign of reduction. The flow rates of these samples are reproducible upon thermal cycling over the entire temperature range of the measurements. Flow rates of samples prepared with gas mixture with  $X_3 = 2 \times 10^{-3}$  and  $1 \times 10^{-2}$  also increase with decreasing temperature but end with an abrupt extinction at respectively 0.1 and 0.12 K. The flow rate of  $X_3 = 3.5 \times 10^{-4}$  shows a significant drop but not a complete extinction near 80 mK. The flow rates of samples showing reduction or extinction near and below 0.1 K are reproducible upon thermal cycling between 0.5 K and 0.15 K. Other than the glaring 100-fold difference in the apparent  $X_3$  for the initial appearance of mass flow extinction the results shown in Fig. 2 resemble those found in the UMass 2 cm samples. It appears a very large fraction of the <sup>3</sup>He atoms is trapped inside the pores of the Vycor glass and the actual  $X_3$  of the 2.5 mm solid samples are many orders of magnitude lower than the  $X_3$  of the starting helium gas. We will show evidence below supporting this conclusion and that the actual  $X_3$  of the 2 cm UMass solid samples are also much lower than the  $X_3$  of the helium gas.

Shear modulus measurements were made in 2007 on solid  $^4\text{He}$  samples of 33 bar with  $X_3$  equal to  $1 \times 10^{-9}$ ,  $8 \times 10^{-8}$ , and  $3 \times 10^{-7}$  [9]. The shear modulus of these samples shows a sigmoid shape enhancement with decreasing temperature. For the  $X_3 = 1 \times 10^{-9}$  sample, the increase begins slowly near 100 mK and then accelerates with decreasing temperature before flattening out below 18 mK. For ease of discussion below, we will identify 100 mK as  $T_S$  for the  $1 \times 10^{-9}$  sample. Similar behaviors are seen for the  $8 \times 10^{-8}$  and  $3 \times 10^{-7}$  samples with  $T_S$  increasing to 180 and 250 mK and the flattening out temperatures increasing to near 22 and 50 mK, respectively. This increase in  $T_S$  with  $X_3$  mirrors the behavior of  $T_d$ , the extinction temperature found in the mass flow measurements. The enhancement in shear modulus was interpreted to be due to the binding of  $^3\text{He}$  atoms on the dislocation lines and a binding energy  $E_D/k_B$  equal to 0.7 K was deduced from this and other experiments [9,10]. The binding or trapping of  $^3\text{He}$  atoms at the nodes or the intersecting points of two or more dislocation lines is energetically more favorable than elsewhere along the dislocation line and hence the binding of  $^3\text{He}$  atoms should begin at the nodes. Therefore,  $T_S$  marks the temperature of the binding of  $^3\text{He}$  atoms at the nodes of the dislocation network. At temperature below  $T_S$ , the continued binding of  $^3\text{He}$  atoms along the dislocation lines shortens the pinning length of the network and accelerates the increase of the shear modulus of the solid. In the low temperature limit, the dislocation lines are saturated with  $^3\text{He}$  and the shear modulus shows a flattening out in value with decreasing temperature.

The trapping of a single  $^3\text{He}$  atom at a dislocation node can block the transport of  $^4\text{He}$  atoms between two connecting superfluid dislocation line segments. When  $n$ , the fraction of nodes with trapped  $^3\text{He}$  atoms in a dislocation network, reaches the percolation limit, i.e., when  $n \geq n_c$ , the superfluid transport along the entire dislocation network will suffer a sudden extinction. If we assume a 3D cubic lattice for the nodes of the dislocation line network,  $n_c$  has been calculated to be  $\sim 0.69$  [11]. We propose the mass flow extinction phenomenon observed at  $T_d$  in the 2 cm and 2.5 mm sample cells is the experimental manifestation of this sharp percolation transition. This mass flow extinction temperature,  $T_d$ , is found near 0.1 K, or about seven times lower than  $E_D/k_B$ . This is the consequence of the much larger configuration space or states available for  $^3\text{He}$  atoms in the solid sample away from the nodes of the dislocation network.

We note that this model of mass flow extinction naturally explains why the phenomenon is not seen in the  $8 \mu\text{m}$  sample cell.  $8 \mu\text{m}$  is shorter than or at most on the order of the typical loop length of dislocation network, which has been deduced from a number of experiments to be between 10 and  $100 \mu\text{m}$  [9,10]. The dislocation lines in  $8 \mu\text{m}$  samples are most likely pinned on the two flat surfaces of the solid disk forming a nearly parallel nonintersecting array that thread through the sample without any intersections or nodes that can trap  $^3\text{He}$  atoms.

If hypothetically mass transport and shear modulus measurements can be conducted simultaneously on a solid sample of a specific  $X_3$ , then mass flow extinction will occur at the same temperature when the shear modulus begins to increase, or  $T_d = T_S$ . In shear modulus measurements,  $X_3$  of the solid

samples, in contrast to those prepared for mass flow measurements, is the same as the  $X_3$  of the helium gas used to grow the solid since there is no coexisting superfluid in the sample cell and the amount of helium in the gaseous phase is minuscule. These observations lead to the conclusion that the  $X_3$  of solid samples that exhibit mass flow extinction at 0.1 K is very close to  $1 \times 10^{-9}$ . The identification of  $T_d$  with  $T_S$  naturally explains why both temperatures increase with increasing  $X_3$ .

What is then the mechanism responsible in depleting the  $X_3$  of the solid samples to the  $1 \times 10^{-9}$  level from the  $X_3$  of the helium gas, 4 and  $10 \times 10^{-6}$  for the 2 cm sample and  $2 \times 10^{-3}$  for the 2.5 mm sample, used to grow the solid samples? At the dilute concentration of interest here,  $^3\text{He}$  atoms are fully miscible in superfluid  $^4\text{He}$  down to 0 K. The solubility of  $^3\text{He}$  in solid  $^4\text{He}$ , however, drops exponentially with temperature below 0.5 K [12]. When the solid and liquid phases are in physical contact as in this experiment, the binding energy of  $^3\text{He}$  atoms in favor of the liquid phase has been calculated to be  $E_L/k_B = 1.36$  K. As a result, the equilibrium ratio of concentrations in solid and liquid,  $X_{3S}/X_{3L}$ , can be calculated to reduce from being close to unity above 0.5 K to  $\sim 10^{-4}$  at 0.1 K [12].

There is an additional reservoir where  $^3\text{He}$  impurities can and will accrue. Three experiments were carried out to study the effect of  $^3\text{He}$  impurities on the various aspects of the  $^4\text{He}$  crystal-superfluid interface. Carmi and his co-workers studied the effect of  $^3\text{He}$  impurities on the roughening transition of the  $c$  facet of  $^4\text{He}$  crystal near 1 K in samples with  $X_3$  between  $8 \times 10^{-7}$  and  $1.5 \times 10^{-4}$ . They found a binding energy  $E_{SL}$  of 10 K that traps a 0.25 monolayer (ML)  $^3\text{He}$  film at the interface [13]. Wang and Agnolet studied the effect of  $^3\text{He}$  impurities on the crystallizing wave along the interface from 30 mK to 0.5 K on samples with  $X_3$  equal to  $4.5 \times 10^{-9}$  and  $1.2 \times 10^{-8}$ . They reported an  $E_{SL}$  of 3.4 K [14]. The surface tension of the interface was measured by Rolley and his colleagues in samples of  $X_3 = 4 \times 10^{-10}$  and  $1.3 \times 10^{-7}$  [15]. The volume of superfluid of their sample cell is  $300 \text{ cm}^3$  and the volume and surface area of the  $^4\text{He}$  crystal are  $10 \text{ cm}^3$  and  $10 \text{ cm}^2$ , respectively. In addition, the sample cell contains a sponge of sintered 40 nm silver particles with a total surface area of  $300 \text{ m}^2$ . Their measurements on the  $X_3 = 1.3 \times 10^{-7}$  sample yield a binding energy  $E_{SL}$  of 4.3 K and they found 0.4 ML  $^3\text{He}$  trapped at the interface. The authors were surprised by the absence of any trapped  $^3\text{He}$  atoms at the interface in the  $X_3 = 4 \times 10^{-10}$  sample in spite of the fact that the total amount of  $^3\text{He}$  in the superfluid is enough to form a 0.3 ML  $^3\text{He}$  film. Although the authors provided another explanation, we think the answer lies with the large surface area of the sintered silver in their sample cell. The first two atomic layers of helium adsorbed onto a substrate such as silver or silica are compressed by the van der Waals potential into an amorphous solid layer. The amorphous solid-superfluid interface should be equally effective in trapping  $^3\text{He}$  as the crystalline solid-superfluid interface. Since the area of this interface is  $300 \text{ m}^2$  or  $3 \times 10^4$  times larger, the number of  $^3\text{He}$  atoms that can be trapped at the crystal-superfluid interface becomes negligible. We note the values of the  $E_{SL}$  found in these three experiments are higher than that calculated by Treiner (at 3 K) [16], and that deduced recently in a recent mass flow measurement at 2.5 K [17].

Similar to Rolley's sample cell, there is an amorphous solid  $^4\text{He}$  layer that coats the silica pore wall of the Vycor glass in the  $SF$ - $S$ - $SF$  sample cells which gives rise to a very large solid-liquid interface. Specifically, the internal pore surface area of the two Vycor rods in the 2.5 mm cell is  $400\text{ m}^2$ . Since the high temperature end of the Vycor glass rods is kept near 1.5 K and the thermal conductivity of porous glass rod even when it is filled with superfluid helium is low [18], the temperature profile of the glass rod has a sigmoid shape; it increases slowly from the temperature of the cell body and then more rapidly before flattening out to 1.5 K. As noted above, when the helium mixture gas is introduced into the sample cell to grow the solid samples, the cell body is kept near 0.5 K. Under this condition, it is reasonable to assume that 25% of the porous glass rod or  $100\text{ m}^2$  of the amorphous solid-superfluid interfacial area will be below 0.75 K and effective in trapping  $^3\text{He}$  atoms. If we assume the trapped  $^3\text{He}$  layer has an areal density of 0.4 ML, then the total number of  $^3\text{He}$  atoms trapped at the solid-liquid interface is  $\sim 4.4 \times 10^{20}$  atoms or  $7.5 \times 10^{-4}$  moles. This number is 10 times larger than all the  $^3\text{He}$  in the  $X_3 = 2 \times 10^{-3}$  mixture gas. Since our protocol in growing solid samples requires all the mixture gas be filtered through the Vycor glass rods, most of the  $^3\text{He}$  impurities are prevented from reaching the solid samples.

When the cell body with the solid sample is cooled from 0.5 K towards  $T_d$  near 0.1 K the following process takes place. In response to the rapidly decreasing solubility,  $^3\text{He}$  atoms in the solid will diffuse into the superfluid in the Vycor until the concentration ratio,  $X_{3S}/X_{3L}$ , is reduced from unity down to  $\sim 10^{-4}$ . In addition, the cooling of the cell body also decreases temperature of the low temperature ends of the Vycor rods and enhances the  $^3\text{He}$  trapping capacity of the solid-liquid interface in Vycor. It requires finite time for  $^3\text{He}$  atoms to diffuse from the solid sample into the superfluid in Vycor during the cooling of the cell body and conversely from superfluid to solid during warming. The diffusion time  $\tau$  of  $^3\text{He}$  impurities over a distance  $l$  in solid  $^4\text{He}$  has been determined by NMR measurements to be independent of temperature below 1 K and proportional to  $X_3$  and  $l^2$  [19]

$$\tau \approx \frac{\langle l \rangle^2}{2} \frac{X_3}{2.6 \times 10^{-11} \text{ cm}^2/\text{s}}. \quad (1)$$

According to Eq. (1),  $\tau$ , the time it takes  $^3\text{He}$  to diffuse through 1.25 mm (half the thickness of the sample) is  $(4 \times 10^8 X_3)$  s. The fact that the measured flow rates shown in Fig. 2 are reproducible upon cooling and warming between 0.1 and 0.5 K indicates the temperature dependent  $X_3$  of the solid sample is keeping up with the changing temperature. This means  $\tau$  is always less than 15 min, the dwell time between data points. This yields an upper limit of  $X_3$  of  $2 \times 10^{-6}$  when we begin to cool the solid sample from 0.5 K. In other words, the great majority of the  $^3\text{He}$  impurities in the gas mixture has indeed been filtered out and trapped in the Vycor glass during the growth of the solid samples. In any case, given the vast capacity of the solid-liquid interface and the superfluid in Vycor in trapping  $^3\text{He}$ , it is not surprising to find that, although  $X_3$  of the starting helium gas is  $2 \times 10^{-3}$ , the actual  $X_3$  of the 2.5 mm sample near 0.1 K is close to  $1 \times 10^{-9}$ .

We can also qualitatively understand why the mass extinction phenomenon observed at UMass is seen in samples made with mixture gas with  $X_3$  equal to  $4 \times 10^{-6}$  and  $1 \times 10^{-5}$  or more than 100 times lower than those growing the 2.5 mm samples. In the UMass experiment, the great majority of the mixture gas is introduced directly into the cell body via a third capillary without being filtered by the two Vycor glass rods. This means the "cleansing" of  $^3\text{He}$  impurities occurs primarily when the sample is being cooled from 0.6 K towards 0.1 K. The total volume of the Vycor rods of the UMass sample cell is 5.7 times smaller and the solid sample is 5.3 times larger than the 2.5 mm cell. If we use the same criteria as the 2.5 mm cell, the total number of  $^3\text{He}$  atoms that can be trapped at the solid-liquid interface in Vycor is  $4.4 \times 10^2$  times more than the total amount of  $^3\text{He}$  atoms in the  $X_3 = 4 \times 10^{-6}$  sample. In other words, it is also not surprising that solid samples made with helium gas with  $X_3 = 4 \times 10^{-6}$  or  $1 \times 10^{-5}$  have a real  $X_3$  close to  $1 \times 10^{-9}$ .

Following the initial cooling scan shown in Fig. 2, five additional warming and cooling scans were made on the  $X_3 = 2 \times 10^{-3}$  sample. These measurements reveal that the mass flow extinction is accompanied by a gradual but complete recovery of the flow rate. Panel (a) of Fig. 3 reproduces the data from the first cooling scan from Fig. 2 together with results from the second (warming) scan over a very narrow temperature range (100 to 140 mK). In contrast to the first cooling scan where mass flow rate was measured at successive lower temperature every 15 min, we took small temperature steps and stay at each temperature much longer in the second scan. The time evolution of the mass flow rate of the second warming scan is shown in panel (a\*) with each data point separated by 15 min. Panel (a\*) begins where the first cooling scan ends with no mass flow at 100 mK. The temperature is then increased to 105 mK after 1 h. At 105 mK a gradual recovery of the mass flow is found; specifically, the mass flow rate grows smoothly with time and saturates after  $\sim 250$  min. Subsequent warming to 110 mK and higher temperatures results in mass flow rates that reproduce the values measured in the first cooling scan. This reproducibility in mass flow rate above  $T_d$  indicates a large fraction of the dislocation nodes are no longer occupied by  $^3\text{He}$  atoms and the dislocation network is fully open to support superfluidlike transport.

We will now turn to the mechanism responsible for the slow recovery of the mass flow observed at 105 mK. In 2012, a shear modulus experiment was carried out to study the time dependence of the stiffness of  $^4\text{He}$  single crystals grown in the presence of a minute amount of  $^3\text{He}$  at low temperature. The crystal is found to be in a stiff state at 23 mK with a time independent shear modulus. It is in the stiff state at this low temperature because the dislocation lines are saturated with  $^3\text{He}$  atoms. When the crystal is warmed to 60 mK, the  $^4\text{He}$  crystal shows a gradual softening over a time interval of 7 h [20]. The authors interpreted this gradual softening to be the consequence of the  $^3\text{He}$  atoms, while being bound on the dislocation lines, migrating and redistributing themselves evenly along the lines. The comparable time scale found in this experiment with the mass flow recovery phenomenon leads us to conclude that we are also observing a migration of  $^3\text{He}$  atoms along the dislocation lines. In the mass flow experiment,  $^3\text{He}$  atoms originally trapped at the intersections



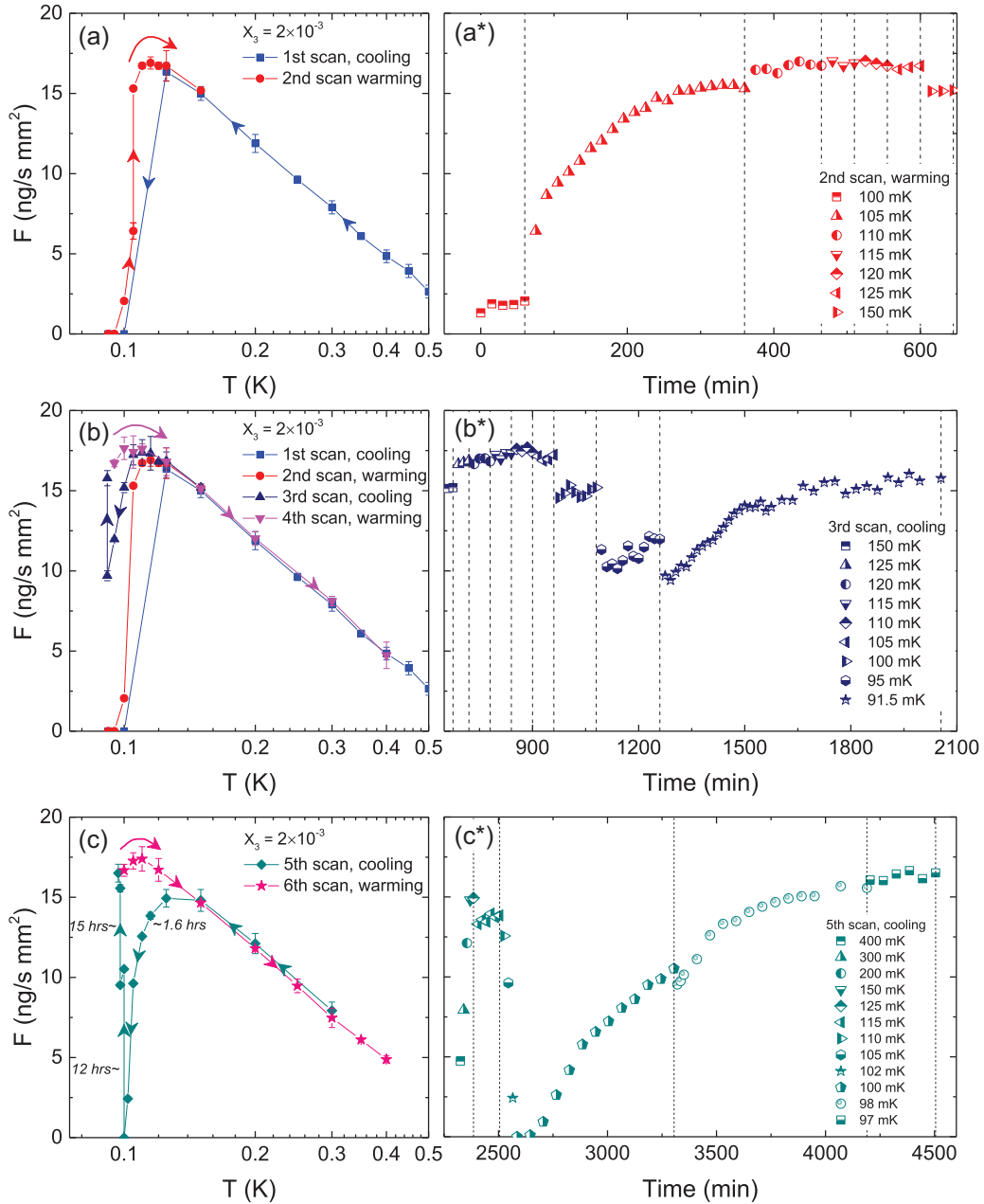


FIG. 3. Mass flow rate of solid sample grown with  $X_3 = 2 \times 10^{-3}$  measured in six sequential cooling and warming scans. These scans show the details of the slow recovery of the mass flow rate. Panels (a)–(c) show mass flow rate as a function of temperature and panels (a\*) to (c\*) show the continuous time evolution of the second (warming), third (cooling), and fifth (cooling) scans.

of the dislocation network slip from the intersections and migrate along the dislocation line into the superfluid in Vycor. Such an “escape” of the  $^3\text{He}$  atoms from the dislocation lines to the superfluid is reasonable in view of the stronger binding energy of  $^3\text{He}$  in superfluid ( $E_L/k_B = 1.36$  K) than on the dislocation line ( $E_D/k_B = 0.7$  K). This gradual migration reduces the fraction of intersections with trapped  $^3\text{He}$  atoms to be below the percolation threshold  $n_c$  and opens up the dislocation network. This slow migration process is very likely always at play but becomes observable in mass flow measurement only when the solid sample is at or near the mass flow extinction temperature  $T = T_d$  when the fraction of dislocation intersections with trapped  $^3\text{He}$  is close to  $n_c$ .

Panels (b) and (b\*) show the results of the third cooling and fourth warming scan. The third cooling scan begins where the second warming scan ends at 150 mK. The most interesting feature of this scan is that instead of a complete shutoff, there is only a reduction in mass flow rate when the solid sample is cooled to 95 mK. This reduction in flow rate is followed by a slow recovery. Further cooling to 91.5 mK results in another sharp drop and then further gradual recovery in the flow rate. The reduction in flow rate at a temperature that is 5 mK below the prior  $T_d$  reflects the reduction of  $X_3$  in the solid during the intervening 800 min. In addition to the continuous diffusion of  $^3\text{He}$  atoms from the solid sample into superfluid to reach the correct temperature dependent  $X_{3S}/X_{3L}$  value, there is also

the slow migration of trapped  $^3\text{He}$  atoms along the dislocation line to the superfluid. With a reduction  $X_3$ , the temperature at which the dislocation nodes are occupied by  $^3\text{He}$  atoms shifts to a lower value. However, with the reduction in  $X_3$ , the number of nodes with  $^3\text{He}$  atoms on the dislocation network may not reach  $n_c$ , the percolation threshold. This results in a reduction instead of an extinction in mass flow. After the reduction, the flow rate shows the usual gradual recovery due to the slow migration of bound  $^3\text{He}$  along the dislocation line to the superfluid. When the temperature is further reduced from 95 to 91.5 mK, the recovery in mass flow is interrupted by another reduction in flow rate due to additional trapping of  $^3\text{He}$  atoms at the nodes of the dislocation network from the solid.

Figure 2 shows that, for the solid sample prepared with mixture gas of  $X_3 = 3.5 \times 10^{-4}$ , the mass flow rate shows a reduction in flow rate near 85 mK without a complete extinction. Similarly, the 2 cm solid sample prepared with helium gas of  $1.7 \times 10^{-7}$  [2] also shows a reduction near 80 mK without a complete extinction. The mechanism responsible for these reductions in mass flow rate should be the same as what we have proposed above for the flow rate reduction seen at 95 and 91.5 mK during the third cooling scan.

Panels (c) and (c\*) show the results of the fifth cooling and the sixth warming scans. The fifth cooling scan starts at 0.4 K, the end point of the fourth warming scan. The most interesting feature of the fifth cooling scan is the reappearance of the extinction of mass flow close to 100 mK. During the warming process to 0.4 K,  $^3\text{He}$  atoms diffuse from the superfluid back to the solid in order to raise the  $X_{3S}/X_{3L}$  value from  $\sim 10^{-4}$  to the expected value of 0.58. The increase in  $X_3$  in the solid raises  $T_d$  back to 100 mK. The shutoff in mass flow found here is not as abrupt as that found in the first cooling scan. This is probably related to the fact in the first cooling scan we cool down the sample from 150 mK to 100 mK in 30 min in two steps, while in the fifth cooling scan, we took 3 h with six temperature steps. With a slower cooling process, the  $X_3$  of the solid sample at intervening

temperatures, particularly between 130 and 100 mK, are more likely to reach the equilibrium value thus allowing for a more gradual pinning of the intersections by  $^3\text{He}$  atoms in the approach to the percolation threshold. After the mass flow extinction at 100 mK, we found again a gradual recovery in the flow rate. However, the recovery rate here is much slower, spanning 30 h. We do not have an explanation why this is so much longer than the 4.2 h found in the second warming scan.

#### IV. SUMMARY

In summary, we replicated the novel  $^3\text{He}$  impurity induced mass flow extinction phenomenon at low temperature in a solid sample of 2.5 mm. In addition, we found a gradual but complete recovery of flow rate after the extinction. We formulated a model that explains all the obvious and also some subtle features of the observed phenomena. Our model attributes the extinction in mass flow to be the consequence of the trapping of  $^3\text{He}$  atoms at the intersections of the dislocation network that blocks the mass transport through the network. When  $n$ , the fraction of intersections with trapped  $^3\text{He}$  atoms, reaches the percolation threshold,  $n_c$ , the mass flow is shut off. The slow recovery of mass flow with a characteristic time of several hours is due to the migration of trapped  $^3\text{He}$  atoms along the dislocation line into the superfluid reservoir. Our model is consistent with the absence of mass flow extinction in 8  $\mu\text{m}$  solid samples because in these thin samples the dislocation lines array has few or no intersections. Since the characteristic time of the recovery phenomenon scales with the dimension of the solid sample, it is likely that the UMass group did not wait long enough to detect it in the 2 cm samples.

#### ACKNOWLEDGMENT

This research is supported by NSF under Grant No. DMR-1707340.

- 
- [1] M. W. Ray and R. B. Hallock, *Phys. Rev. Lett.* **100**, 235301 (2008); **105**, 145301 (2010); Y. Vekhov and R. B. Hallock, *ibid.* **109**, 045303 (2012).
- [2] Ye. Vekhov, W. J. Mullin, and R. B. Hallock, *Phys. Rev. Lett.* **113**, 035302 (2014); Ye. Vekhov and R. B. Hallock, *Phys. Rev. B* **92**, 104509 (2015).
- [3] R. B. Hallock, *J. Low Temp. Phys.* **197**, 167 (2019).
- [4] M. Boninsegni, A. B. Kuklov, L. Pollet, N. V. Prokof'ev, B. V. Svistunov, and M. Troyer, *Phys. Rev. Lett.* **99**, 035301 (2007).
- [5] S. G. Soyler, A. B. Kuklov, L. Pollet, N. V. Prokof'ev, and B. V. Svistunov, *Phys. Rev. Lett.* **103**, 175301 (2009).
- [6] J. Shin, D. Y. Kim, A. Hazirot, and M. H. W. Chan, *Phys. Rev. Lett.* **118**, 235301 (2017).
- [7] J. Shin and M. H. W. Chan, *Phys. Rev. B* **99**, 140502(R) (2019).
- [8] Z. G. Cheng and J. Beamish, *Phys. Rev. Lett.* **117**, 025301 (2016).
- [9] J. Day and J. Beamish, *Nature (London)* **450**, 853 (2007).
- [10] A. D. Fefferman, F. Souris, A. Hazirot, J. R. Beamish, and S. Balibar, *Phys. Rev. B* **89**, 014105 (2014).
- [11] M. F. Sykes and J. W. Essam, *Phys. Rev.* **133**, A310 (1964).
- [12] D. O. Edwards and S. Balibar, *Phys. Rev. B* **39**, 4083 (1989); C. Pantalei, X. Rojas, D. O. Edwards, H. J. Maris, and S. Balibar, *J. Low Temp. Phys.* **159**, 452 (2010).
- [13] Y. Carmi, E. Polturak, and S. G. Lipson, *Phys. Rev. Lett.* **62**, 1364 (1989).
- [14] C.-L. Wang and G. Agnolet, *J. Low Temp. Phys.* **89**, 759 (1992).
- [15] E. Rolley, S. Balibar, C. Guthmann, and P. Nozières, *Phys. B (Amsterdam, Neth.)* **210**, 397 (1995).
- [16] J. Treiner, *J. Low Temp. Phys.* **92**, 1 (1993).
- [17] Z. G. Cheng, J. Beamish, A. D. Fefferman, F. Souris, S. Balibar, and V. Dauvois, *Phys. Rev. Lett.* **114**, 165301 (2015).
- [18] Z. G. Cheng and M. H. W. Chan, *New J. Phys.* **15**, 063030 (2013).
- [19] A. Allen, M. Richards, and J. Schratte, *J. Low Temp. Phys.* **47**, 289 (1982); J. Schratte, A. Allen, and M. Richards, *ibid.* **57**, 179 (1984).
- [20] X. Rojas, A. Hazirot, and S. Balibar, *J. Phys.: Conf. Ser.* **400**, 012062 (2012).

*Correction:* The ORCID identifier for the second author was presented incorrectly and has been fixed.